AGU PUBLICATIONS

Geophysical Research Letters

RESEARCH LETTER

10.1002/2014GL059788

Key Points:
- Quasi-neutral hybrid simulation of lunar magnetic anomaly-solar wind interaction
- Formation of antimoonward Hall electric field at lunar magnetic anomaly
- Hall electric field results in potential wall even without charge separation

Correspondence to:
R. Jarvinen,
riku.jarvinen@fmi.fi

Citation:
Jarvinen, R., M. Alho, E. Kallio, P. Wurz, S. Barabash, and Y. Futaana (2014), On vertical electric fields at lunar magnetic anomalies, *Geophys. Res. Lett.*, *41*, 2243–2249, doi:10.1002/2014GL059788.

Received 3 MAR 2014
Accepted 21 MAR 2014
Accepted article online 25 MAR 2014
Published online 2 APR 2014

On vertical electric fields at lunar magnetic anomalies

R. Jarvinen[1,2], M. Alho[1], E. Kallio[1,3], P. Wurz[4], S. Barabash[5], and Y. Futaana[5]

[1]Finnish Meteorological Institute, Helsinki, Finland, [2]Laboratory for Atmospheric and Space Physics, University of Colorado Boulder, Boulder, Colorado, USA, [3]School of Electrical Engineering, Aalto University, Helsinki, Finland, [4]Physikalisches Institut, University of Bern, Bern, Switzerland, [5]Swedish Institute of Space Physics, Kiruna, Sweden

Abstract We study the interaction between a magnetic dipole mimicking the Gerasimovich magnetic anomaly on the lunar surface and the solar wind in a self-consistent 3-D quasi-neutral hybrid simulation where ions are modeled as particles and electrons as a charge-neutralizing fluid. Especially, we consider the origin of the recently observed electric potentials at lunar magnetic anomalies. An antimoonward Hall electric field forms in our simulation resulting in a potential difference of <300 V on the lunar surface, in which the value is similar to observations. Since the hybrid model assumes charge neutrality, our results suggest that the electric potentials at lunar magnetic anomalies can be formed by decoupling of ion and electron motion even without charge separation.

1. Introduction

The Moon does not have a global intrinsic magnetic field, but it has local magnetized regions on its surface [*Richmond and Hood*, 2008]. The magnetic pressure associated with these magnetic anomalies can exceed the dynamic pressure of the solar wind. It has been argued that spatially small magnetospheres or "minimagnetospheres" may be formed around the lunar magnetic anomalies [*Lin et al.*, 1998].

Recent ion, electron, and energetic neutral atom (ENA) observations from spacecraft orbiting the Moon suggest that there exists an upward (antimoonward) electric field within magnetic anomaly regions on the lunar surface resulting in a vertical potential difference, which we refer to as "the potential wall" in this study. *Saito et al.* [2012] analyzed ion and electron observations from the Kaguya spacecraft above the South Pole Aitken region and found potentials of 150 V above the ~25 km altitude. The Chandrayaan-1 ENA observations were used to deduce the >135 V electric potential values in the isolated magnetic anomaly near the Gerasimovich crater in a study by *Futaana et al.* [2013].

The physics of electric fields near the lunar surface is rich in plasma phenomena and includes spatial scales of several orders of magnitude, ranging from Debye lengths to ion gyroradii [e.g., *Kallio et al.*, 2012]. For example, *Wang et al.* [2012, 2013] identified potential structures related to the surface charging in a laboratory study using a magnetic dipole and a plasma flow with unmagnetized protons and magnetized electrons. *Shaikhislamov et al.* [2013, 2014] studied laboratory measurements and a Hall-MHD simulation arguing that the Hall term of the electric field may play an important role in decoupling the ion and electron flow in lunar minimagnetospheres. Self-consistent fluid simulations predict the formation of lunar minimagnetospheres around the strongest lunar magnetic anomalies [e.g., *Harnett and Winglee*, 2000].

It is crucial to understand the nature of the electric fields and potentials at the magnetic anomalies to quantify the dynamics of charged particles near the lunar surface.

In this study we use a three-dimensional (3-D) hybrid simulation model to study the interaction between a magnetic dipole and the solar wind. Special emphasis is placed to analyze the electric field and the potentials formed in the interaction.

The study is organized as follows. In the next section we describe the model used. Then we present the simulation results. At the end we discuss and summarize our findings.

2. Model

The simulation model used in this work is the 3-D HYB hybrid simulation platform developed at the Finnish Meteorological Institute. The advantage of the hybrid approach is that it includes ion kinetic effects, and ion

velocity distributions evolve according to the model calculation as ions are modeled as particles. The ion dynamics are self-consistently coupled with the electric and magnetic field. Next we summarize the most important features of the HYB-Anomaly model for this study (see details in *Kallio et al.* [2012]).

In the model the solar wind H^+ ions are treated as particles moving under the Lorentz force:

$$m_p \mathrm{d}\vec{v}_i/\mathrm{d}t = e(\vec{E} + \vec{v}_i \times \vec{B}), \tag{1}$$

where m_p is the proton mass, $\vec{v}_i$ is the ion velocity, e is the positive elementary charge, $\vec{E}$ is the electric field, and $\vec{B}$ is the magnetic field. Electrons are modeled as a massless, charge-neutralizing fluid, and their velocity is defined as

$$\vec{U}_\mathrm{e} = \vec{U}_{\mathrm{H}^+} - \vec{J}/(en) = \vec{U}_{\mathrm{H}^+} - \nabla \times \vec{B}/(\mu_0 en), \tag{2}$$

where $\vec{U}_{\mathrm{H}^+}$ is the ion bulk velocity; $\vec{J}$ is the electric current density defined by Amperè's law; n is the electron number density, which according to the quasi-neutrality assumption of the model equals the proton number density; and μ_0 is the magnetic vacuum permeability. A notable feature in equation (2) is that the ion and electron flows are not the same if electric currents exist even though the charge neutrality is assumed in the model.

The magnetic field is propagated by Faraday's law in a Cartesian simulation mesh of cubic grid cells. In Faraday's law a finite, constant resistivity term of the electric field was used to include some magnetic field diffusion in the simulation.

The electric field is defined in the simulation as

$$\vec{E} = -\vec{U}_\mathrm{e} \times \vec{B} = \underbrace{-\vec{U}_{\mathrm{H}^+} \times \vec{B}}_{\vec{E}_\mathrm{conv}} + \underbrace{\frac{\vec{J} \times \vec{B}}{en}}_{\vec{E}_{J\times B}}. \tag{3}$$

We call the first term the ion convection term ($\vec{E}_\mathrm{conv}$) and the second term the Hall $\vec{J} \times \vec{B}$ term ($\vec{E}_{J\times B}$).

Equation (3) is a simplified version of the full momentum equation, which includes, for example, the electron pressure term. However, the electron pressure of isothermal electrons was found to be not important for the results of this study in our test runs. Further, note that equation (3) is derived assuming massless electrons, while the ion inertia is included in the model (equation (1)). Equation (3) states that the properties of the magnetic field are associated ("frozen in") with the electron motion. On the other hand, the ion motion determines the "mass flow" in the model.

2.1. Coordinate System

The Cartesian coordinate system used in the model is defined as follows. The incident solar wind flow is along the negative x axis, the anomaly dipole moment is along the z axis, and the y axis completes the right-handed coordinate system. The origin is on the lunar surface directly above the dipole, and the simulation box is horizontally centered around the origin.

2.2. Simulation Setup

A magnetic dipole mimicking the Gerasimovich anomaly is placed in the simulation at $\vec{r} = (x = -50$ km), $(y = 0, z = 0)$ under the surface with the surface magnitude of 96 nT along the x axis (23 nT at $x = 30$ km and 1 nT at $x = 200$ km) (the same as in our earlier study [*Kallio et al.*, 2012]). The anomaly orientation is such that the dipole field is directed along the negative z axis, which is opposite to the undisturbed interplanetary magnetic field (IMF) in the origin. An incident solar wind speed of 300 km s^{-1} was chosen to correspond to the case analyzed by *Futaana et al.* [2013]. The surface is treated as a particle-absorbing plane at $x = 0$. Electric charging is not included in the hybrid model. The magnetic field is assumed to penetrate in the surface undisturbed. That is, the Moon is assumed to be an ideal insulator. See Table 1 for a list of parameters of the simulation run.

3. Simulation Results

Figure 1 illustrates the magnetic field and the proton flow in the simulation. Above $x \sim 100$ km the magnetic field lines are the IMF field lines convecting toward the magnetic anomaly with the incident solar wind.

Table 1. Details and Upstream Solar Wind (SW) Conditions of the HYB-Anomaly Simulation Run Analyzed in This Work

Parameter	Value
Box size ($x \times y \times z$) (km)	$(0...200) \times (-200...200) \times (-200...200)$
Number of grid cells ($n_x \times n_y \times n_z$)	$30 \times 60 \times 60$
Grid cell size (Δx^3)	$(20/3\,\mathrm{km})^3 \approx (6.7\,\mathrm{km})^3$
Average macroparticles per cell	30
Time step (Δt)	0.11 ms
Solution snapshot time	6.2 s
IMF $\vec{B}_{sw}$	$[B_x, B_y, B_z] = [0, 0, 6]$ nT
SW $\vec{E}_{sw}$	$[E_x, E_y, E_z] = [0, -1.8, 0]$ mV m^{-1}
SW H^+ velocity $\vec{U}_{sw}$	$[U_x, U_y, U_z] = [-300, 0, 0]$ km s^{-1}
SW H^+ n and T	10 cm^{-3}, 76,000 K

Below $x \sim 100$ km the magnetic field lines either connect to the IMF or the lunar surface. The "closed" magnetic field lines connected to the surface at both ends are centered around the origin. The surface connection of the "open" field lines occurs at the z axis at around $z = \pm 50$ km in the polar region of the anomaly dipole field (black contours in Figure 1). Also, a notable feature in Figure 1 is that the proton flow is vertical almost everywhere.

Figure 2 analyzes the electric field and the electric current. At $x \leq 50$ km a horizontal electric current system (J_{hor}) occurs where the current flows along the negative y axis in the middle ($z = 0$) and circles the polar regions of the anomaly dipole field in the $z < 0$ and $z > 0$ hemispheres. Also, the magnitude of the electric field at $x < 30$ km is higher near the origin than in the area surrounding the magnetic anomaly.

Figure 3 displays the electric field at $x = 10$ km separately for the full electric field, the Hall term, and the ion convection term (equation (3)). Further, the electric field is shown separately for the total, vertical, and horizontal components.

Two different regions can be identified in the total electric field (Figure 3a): The horizontal electric field (the solar wind convection electric field) dominates outside of the center of the anomaly region ($\sqrt{y^2+z^2} \gtrsim 50$ km), and the vertical (Hall) electric field dominates in the central anomaly region ($\sqrt{y^2+z^2} \lesssim 50$ km). In Figures 3d–3f it can be seen that the strongest positive vertical fields occur at ($\sqrt{y^2+z^2} \lesssim 50$ km). At $\sqrt{y^2+z^2} \gtrsim 50$ km there is no visible vertical electric field (Figure 3d). Overall, the vertical component of the electric field is a result of the Hall term, whereas the convection term does not contribute to the vertical electric field (Figure 3e versus Figure 3f).

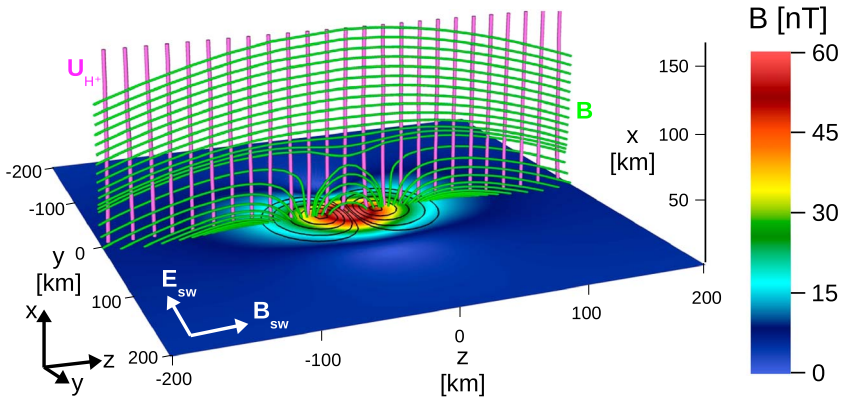

Figure 1. Magnetic field and solar wind proton flow in the HYB-Anomaly hybrid simulation. The color map gives the magnitude of the magnetic field on the surface. The black contours are the isocontours of B_x on the surface. The vertical magenta lines are the bulk flow streamlines of the solar wind protons. Green lines are the magnetic field lines. The field line tracing was started at altitudes below 150 km.

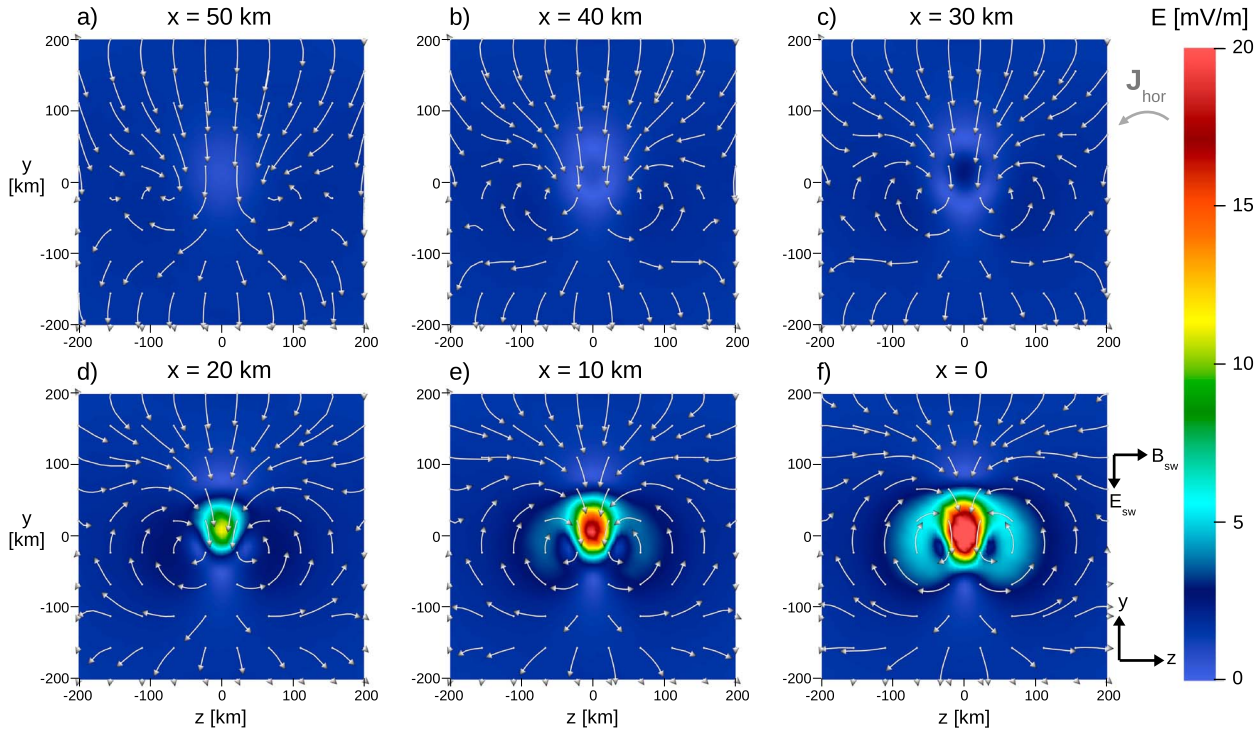

Figure 2. Horizontal (*yz*) cuts of a lunar magnetic anomaly in the HYB-Anomaly hybrid simulation at $x = 0...50$ km altitudes. The color map shows the magnitude of the electric field, and the curved gray arrows give the morphology of the horizontal component of the electric current density.

Figure 4 studies the altitude dependence of the electric potential. The potential is defined along the direction of the undisturbed solar wind flow (the *x* axis), and it is referred to as the anomaly potential (ϕ_a) in this study:

$$\phi_a(\vec{r}_p) \equiv \int_{\vec{r}_{sw}}^{\vec{r}_p} \vec{E}(\vec{r}) \cdot d\vec{r} + \phi(\vec{r}_{sw}), \tag{4}$$

where $\vec{r}_{sw}$ is a point in the undisturbed solar wind at $x = 200$ km (the inflow boundary), $\vec{r}_p$ is a point on the shown *yz* plane in the figure, and the displacement vector $d\vec{r}$ is along $\vec{U}_{sw}$ (the *x* axis). The potential in the undisturbed solar wind is taken to be zero $\phi(\vec{r}_{sw}) = \text{constant} = 0$.

Equation (4) defines ϕ_a such that it is constant (set as zero here) along a flow line in the undisturbed solar wind. Thus, changes in ϕ_a are associated with the electric field disturbances caused by the magnetic anomaly. If a proton moves exactly along $\vec{U}_{sw}$, the change in ϕ_a is directly related to the change of the proton kinetic energy according to the conservation of energy in a stationary situation.

From Figure 4 it can be seen that positive ϕ_a values start to occur at around the altitude of $x = 20$ km in the central anomaly region within $\sqrt{y^2 + z^2} \lesssim 50$ km. The anomaly potential reaches its maximum of around 300 V on the surface near the origin. Further, the anomaly potential increases with decreasing altitude indicating that the upward pointing electric field is a general feature within the anomaly and not constrained to the $x = 10$ km surface as one might infer from Figure 3.

4. Discussion

We modeled the interaction between a lunar dipolar magnetic anomaly and the solar wind in a self-consistent 3-D hybrid simulation. Especially, we analyzed the electric fields and the electric potential created in the interaction.

In Figures 3d–3f it was seen that the Hall term dominates the antimoonward vertical electric field. What causes this Hall field? According to equation (3) vertical Hall field arises when the $\vec{J} \times \vec{B}$ cross product is along the *x* axis. This situation occurs since the magnetic field is mostly horizontal in the simulation except in the dipole polar regions (Figure 1), and there exists a horizontal current (see J_{hor} in Figure 2).

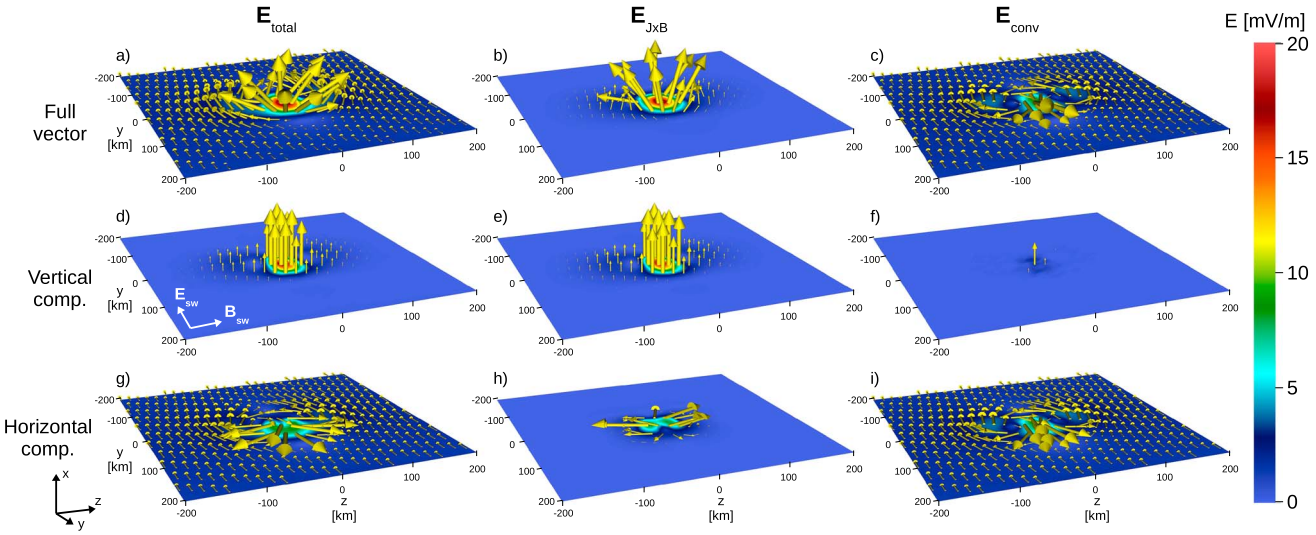

Figure 3. Properties of the electric field at $x = 10$ km in the HYB-Anomaly hybrid simulation. (left) The total electric field, (middle) the Hall electric field, and (right) the ion convection electric field (equation (3)). (a–c) The full electric field vector, (d–f) the vertical (x) component, and (g–i) the horizontal (yz) component. The color map gives the magnitude of the electric field term and component in question. The yellow arrows are the vectors of the electric field term and component in question. The arrow length is linearly proportional to the vector magnitude, but the maximum displayed vector arrow length is 6 mV m^{-1} to clarify the illustration. All the color maps and vectors are at the same scale in the figure. The viewing angle in the plots is the same as in Figure 1.

Note that the horizontal component of the Hall field is also strong near the polar regions of the anomaly (Figure 3h) where the magnetic field turns vertical (black contours in Figure 1). Vertical $\vec{B}$ and J_{hor} in these regions result in the $\vec{J} \times \vec{B}$ cross product in the horizontal direction.

In the simulation the magnetic field is mostly horizontal because of the chosen IMF and dipole orientations, but why does J_{hor} that circles the dipole polar regions occur? To the first order the formation of this current system can be understood as a result of an undisturbed solar wind proton flow across a magnetic dipole field ($\vec{B}_{dipole}$). According to the $-\vec{U}_{sw} \times \vec{B}_{dipole}$ expression (equation (3)), the undisturbed $\vec{U}_{sw}$ across $\vec{B}_{dipole}$ gives rise to a "two-pole" pattern in the convection electric field (E_{conv}) circling the dipole poles in $z > 0$ and $z < 0$ hemispheres similar to what is seen in Figures 3c and 3i. E_{conv} is weak in the dipole polar regions because $\vec{B}$ and $\vec{U}_{H^+}$ are aligned (vertical) there, and E_{conv} is the strongest near the x axis since B is the strongest there. Further, E_{conv} in Faraday's law results in the creation of a "two-pole" horizontal magnetic field, which is associated with J_{hor} (Figure 2) via Amperè's law.

The decoupling of ions and electrons allows the electrons to carry J_{hor}, whereas proton motion is mostly vertical. If the Hall term is neglected in the electric field (equation (3)) and, thus, the electrons are forced to flow with the ions, no J_{hor} occurs.

Why is there no formation of a "magnetopause" in the studied simulation case? In a fluid description the pressure balance between the solar wind dynamic pressure and the dipole magnetic pressure along the x axis reads as follows: $m_p n_{sw} U_{sw}^2 = B^2/(2\mu_0)$. The dynamic pressure of the undisturbed solar wind is equal to the magnetic pressure of a ~62 nT field in our simulation case. This magnitude of the dipole field exists at the altitude of $x \sim 8$ km, which we refer to as the "pressure balance altitude." The gyroradius of an H^+ ion moving at 300 km s^{-1} perpendicular to the 62 nT field is 51 km, which is much larger than the pressure balance altitude. Thus, the solar wind protons are not stopped at the pressure balance altitude but impact in the surface due to their large gyroradii, and there is no formation of a "minimagnetosphere magnetopause" boundary.

Since the ion flow is not stopped nor diverted much inside the magnetic anomaly field, there is no formation of an ion cavity for the chosen plasma parameters. A study analyzing two fly-throughs of a strong magnetic anomaly by Lunar Prospector showed that the formation of an ion cavity may be rare in lunar magnetic anomalies [*Halekas et al.*, 2008].

Even though the bulk flow of the solar wind protons is not stopped by the dipole field, small parts of protons are deflected by the magnetic anomaly even in the present simulation case (see an example in *Kallio et al.*

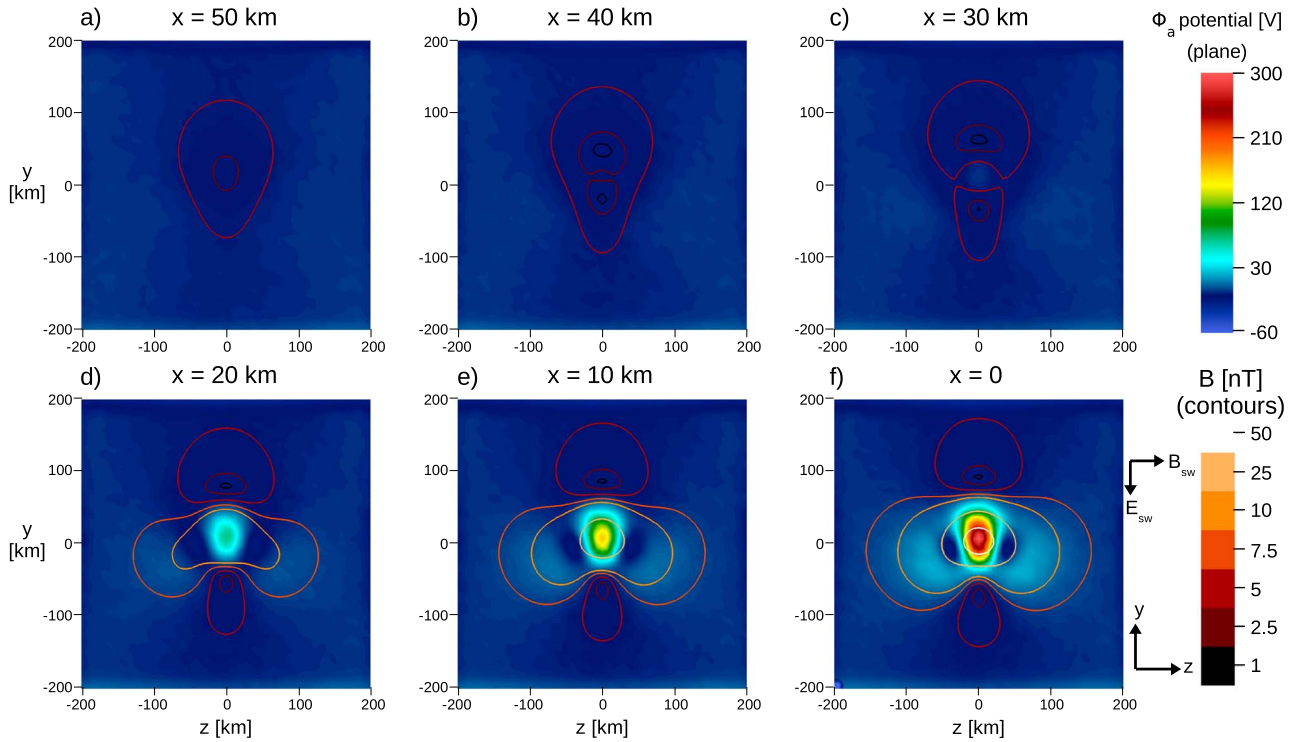

Figure 4. Horizontal (*yz*) cuts of the effective electric potential in the HYB-Anomaly hybrid simulation at $x = 0...50$ km altitudes. The color map gives the anomaly potential ϕ_a defined in equation (4), and the isocontours give the magnitude of the magnetic field. Otherwise the figure is in the same format as Figure 2.

[2012, Figure 3b]). Further, the solar wind protons impacting the surface in the central anomaly region lose energy when they move toward the antimoonward Hall field. Efficient ion deflection from lunar magnetic anomalies was observed recently by Sub-keV Atom Reflecting Analyzer (SARA) on Chandrayaan-1 [*Lue et al.*, 2011], however, in a geometry with nonnormal incidence of the solar wind ions. Also, ENA data in studies by *Wieser et al.* [2010] and *Vorburger et al.* [2012] show that a fraction of ions are deflected from the anomaly for a nonnormal incidence geometry and that the anomalies slow down the solar wind protons resulting in lower ENA energies than the incident solar wind proton energies.

There are several open questions about plasma physics of the lunar magnetic anomalies. First, near the surface, electron kinetics and surface charging play an important role in creating electric field within the Debye sheath [see, e.g., *Kallio et al.*, 2012; *Wang et al.*, 2012, 2013]. Fully kinetic simulations, where both ions and electrons are treated as particles, and plasma and surface charging are included, are called for to further study the nature of the electric fields at the lunar magnetic anomalies within the Debye sheath. Second, the simulation run studied here was carried out for a perpendicular solar wind with respect to the lunar surface, which corresponds to the solar zenith angle of 0°. Most of the time the magnetic anomaly is not in the subsolar point. In that case, the interaction becomes more complicated due to the smaller than 90° angle between the solar wind and the lunar surface. Further, the orientation of the magnetic anomaly in this study was the same as in our earlier work [*Kallio et al.*, 2012], but different orientations can result in different kinds of solar wind interactions [*Wang et al.*, 2013]. In our test runs the orientation of the IMF in the perpendicular direction to the undisturbed solar wind flow (the IMF clock angle) did not affect notably the results concluded here.

5. Summary

We have studied the interaction between a magnetic dipole mimicking the Gerasimovich magnetic anomaly on the lunar surface and the solar wind in a self-consistent 3-D quasi-neutral hybrid simulation where ions are modeled as particles and electrons as a charge-neutralizing fluid. Especially, we considered the origin of the recently observed electric potentials at lunar magnetic anomalies. An antimoonward Hall electric field formed in our simulation resulting in a potential difference of <300 V on the lunar surface, in which the value

is similar to recent observations [*Saito et al.*, 2012; *Futaana et al.*, 2013]. Since the hybrid model assumes charge neutrality, our results suggest that the electric potentials at lunar magnetic anomalies can be formed by decoupling of ion and electron motion even without charge separation.

Acknowledgments
The work of the lead author was supported by the Academy of Finland. All figures were created using the VisIt open source visualization tool.

The Editor thanks Mihaly Horanyi and an anonymous reviewer for their assistance in evaluating this paper.

References

Futaana, Y., S. Barabash, M. Wieser, C. Lue, P. Wurz, A. Vorburger, A. Bhardwaj, and K. Asamura (2013), Remote energetic neutral atom imaging of electric potential over a lunar magnetic anomaly, *Geophys. Res. Lett.*, *40*, 262–266, doi:10.1002/grl.50135.

Halekas, J. S., G. T. Delory, D. A. Brain, R. P. Lin, and D. L. Mitchell (2008), Density cavity observed over a strong lunar crustal magnetic anomaly in the solar wind: A mini-magnetosphere? *Planet. Space Sci.*, *56*, 941–946, doi:10.1016/j.pss.2008.01.008.

Harnett, E. M., and R. Winglee (2000), Two-dimensional MHD simulation of the solar wind interaction with magnetic field anomalies on the surface of the Moon, *J. Geophys. Res.*, *105*, 24,997–25,008, doi:10.1029/2000JA000074.

Kallio, E., et al. (2012), Kinetic simulations of finite gyroradius effects in the lunar plasma environment on global, meso, and microscales, *Planet. Space Sci.*, *74*, 146–155, doi:10.1016/j.pss.2012.09.012.

Lin, R. P., D. L. Mitchell, D. W. Curtis, K. A. Anderson, C. W. Carlson, J. McFadden, M. H. Acuna, L. L. Hood, and A. Binder (1998), Lunar surface magnetic fields and their interaction with the solar wind: Results from Lunar Prospector, *Science*, *281*, 1480–1484, doi:10.1126/science.281.5382.1480.

Lue, C., Y. Futaana, S. Barabash, M. Wieser, M. Holmström, A. Bhardwaj, M. B. Dhanya, and P. Wurz (2011), Strong influence of lunar crustal fields on the solar wind flow, *Geophys. Res. Lett.*, *38*, L03202, doi:10.1029/2010GL046215.

Richmond, N. C., and L. L. Hood (2008), A preliminary global map of the vector lunar crustal magnetic field based on Lunar Prospector magnetometer data, *J. Geophys. Res.*, *113*, E02010, doi:10.1029/2007JE002933.

Saito, Y., M. N. Nishino, M. Fujimoto, T. Yamamoto, S. Yokota, H. Tsunakawa, H. Shibuya, M. Matsushima, H. Shimizu, and F. Takahashi (2012), Simultaneous observation of the electron acceleration and ion deceleration over lunar magnetic anomalies, *Earth Planets Space*, *64*, 83–92, doi:10.5047/eps.2011.07.011.

Shaikhislamov, I. F., V. M. Antonov, Y. P. Zakharov, E. L. Boyarintsev, A. V. Melekhov, V. G. Posukh, and A. G. Ponomarenko (2013), Mini-magnetosphere: Laboratory experiment, physical model and Hall MHD simulation, *Adv. Space Res.*, *52*, 422–436, doi:10.1016/j.asr.2013.03.034.

Shaikhislamov, I. F., Y. P. Zakharov, V. G. Posukh, A. V. Melekhov, V. M. Antonov, E. L. Boyarintsev, and A. G. Ponomarenko (2014), Experimental study of a mini-magnetosphere, *Plasma Phys. Controlled Fusion*, *56*(2), 025004, doi:10.1088/0741-3335/56/2/025004.

Vorburger, A., P. Wurz, S. Barabash, M. Wieser, Y. Futaana, M. Holmström, A. Bhardwaj, and K. Asamura (2012), Energetic neutral atom observations of magnetic anomalies on the lunar surface, *J. Geophys. Res.*, *117*, A07208, doi:10.1029/2012JA017553.

Wang, X., M. Horányi, and S. Robertson (2012), Characteristics of a plasma sheath in a magnetic dipole field: Implications to the solar wind interaction with the lunar magnetic anomalies, *J. Geophys. Res.*, *117*, A06226, doi:10.1029/2012JA017635.

Wang, X., C. T. Howes, M. Horányi, and S. Robertson (2013), Electric potentials in magnetic dipole fields normal and oblique to a surface in plasma: Understanding the solar wind interaction with lunar magnetic anomalies, *Geophys. Res. Lett.*, *40*, 1686–1690, doi:10.1002/grl.50367.

Wieser, M., S. Barabash, Y. Futaana, M. Holmström, A. Bhardwaj, R. Sridharan, M. B. Dhanya, A. Schaufelberger, P. Wurz, and K. Asamura (2010), First observation of a mini-magnetosphere above a lunar magnetic anomaly using energetic neutral atoms, *Geophys. Res. Lett.*, *37*, L05103, doi:10.1029/2009GL041721.